Chapter 1

Projectile electron spectroscopy and new answers to old questions: Latest results at the new atomic physics beamline in Demokritos, Athens

I. Madesis[1,3], A. Laoutaris[1,3], T.J.M. Zouros[1,3*], S. Nanos[2] and E.P. Benis[2]

[1] *Department of Physics, University of Crete, Voutes University Campus, GR-70013 Heraklion, Crete, Greece*

[2] *Department of Physics, University of Ioannina, GR-45110 Ioannina, Greece*

[3] *Tandem Accelerator Laboratory, Institute of Nuclear and Particle Physics, National Center for Scientific Research "Demokritos", GR-15310 Aghia Paraskevi, Greece*

A new experimental station has been setup at the Athens 5.5 MV tandem accelerator to perform zero-degree Auger projectile electron spectroscopy (ZAPS). In addition, two systems of gas and foil terminal- and post-strippers have also been installed to vary the metastable $1s2s\,^3S$ beam component in the He-like ion beams. After a short introduction to the ZAPS technique and our new experimental station, we present new results on the production of the $C^{3+}(1s2s2p\,^{2,4}P, 1s2p^2\,^2D)$ and $C^{4+}(2s2p\,^{3,1}P)$ states in collisions of mixed $C^{4+}(1s2s\,^3S,\ 1s^2)$ ions with He. The $2s2p\,^{3,1}P$ states can be produced by direct $1s \rightarrow 2p$ excitation, electron-electron interaction plus spin exchange and/or transfer-loss processes. The $1s2s2p$ states can be produced either by direct electron capture to the $1s2s\,^3S$ component or by transfer-excitation from the $1s^2$ ground state. A new technique allows for the separate determination of the contributions from the ground and metastable beam components. The ratio $R_m = \sigma_m(^4P)/\sigma_m(^2P)$ of transfer to the metastable component leading to the production of the $^4P,^2P$ states is determined and compared to other older measurements on B^{3+} and F^{7+} similarly analyzed, giving $R_m \simeq 2$ in agreement with spin statistics. No convincing evidence of cascade feeding of the $1s2s2p\,^4P$ state is found, in clear dis-

*Corresponding author. Email: tzouros@physics.uoc.gr

agreement with previous experimental and theoretical results. Clearly, more work is needed to resolve this puzzle.

Contents

1. Introduction

Over the last few decades, considerable progress has been made to obtain information on both the atomic structure and collision dynamics of multiply excited atomic states using high resolution Auger electron spectroscopy [1, 2]. This interest has been generated to a large degree in the fields of plasma physics, thermonuclear fusion research, astrophysics and radiotherapy with light ions (hadron therapy) [3], where the collisional properties of highly stripped ions play an important role. The determination of highly accurate excitation energies, transition rates and lifetimes combined with production cross section information obtained from line intensity measurements lead to a better overall understanding of the dominant processes at play.

The technique of zero-degree Auger projectile electron spectroscopy (ZAPS), described next, has been highly successful in enabling measurements of LS-resolved cross sections as a function of collision energy. The

ZAPS technique offers an experimental window, particularly for ions with low projectile atomic number (Z_p) where the Auger yields are more favorable, for an improved understanding of ion-atom collision mechanisms at the state-selective level and provides stringent testing of theory.

A state-of-the-art ZAPS experimental station has recently been setup in the Athens 5.5 MV tandem Van de Graaff accelerator (TANDEM) at the National Center for Scientific Research "Demokritos" under the Atomic physics with accelerators: projectile electron spectroscopy (APAPES) [4] initiative. Recent progress and new results are presented here.

2. The technique of zero-degree Auger projectile spectroscopy

High resolution Auger projectile spectroscopy refers to the experimental energy- and angular-resolved electron spectroscopic technique in which Auger electrons ejected from a moving emitter (usually a projectile ion beam) are energy analyzed and detected at or close to the observation angle $\theta = 0°$ with respect to the beam direction. This technique is, therefore, known as ZAPS [1].

The ZAPS technique refers mostly to high energy resolution ($< 0.5\%$) measurements of Auger KLL electrons with characteristic energies in the range of 50-600 eV (in the projectile rest frame). It also includes electrons emitted in autoionization, autodetachment as well as photo-ionization processes of ions. In the future, ZAPS could possibly include even high energy [5] conversion [6–8] and beta-electron [9, 10] emission processes measured by magnetic zero-degree spectrometers. All these emitted electrons have characteristic energies and, therefore, carry important atomic structure information such as state energy, binding energy, line width, etc. The particular laboratory detection angle of $\theta = 0°$ offers the optimal kinematic conditions for attaining the highest possible resolution. Equally important, within the category of state-selective measurements, the ZAPS technique also allows for the determination of LS-resolved electron production cross sections. This provides important information about the projectile dynamics in atomic collisions, such as single electron capture, a process of primary interest to the APAPES [4] investigations.

2.1. *Kinematics of fast emitters*

Since the measured electrons are emitted from fast projectile ions, it is important to understand some of the basics of projectile electron kinematics.

A detailed analysis can be quite complicated [11]. However, in the case of energetic collisions of a few MeV/u or more, projectile ions are scattered through very small angles (~mrads) resulting in negligible energy loss and influence on the projectile trajectory. Thus, a simple velocity vector addition model is sufficient for the determination of most kinematic effects [1]. The velocity $\boldsymbol{v}$ of the Auger electron in the laboratory frame is obtained by adding the projectile velocity $\boldsymbol{V}_p$ to the velocity $\boldsymbol{v}'$ of the electron in the projectile rest frame, as shown in Fig. 1. Using the notation with primed quantities in the projectile rest frame, the electron kinetic energy ε in the laboratory frame can be related to the corresponding rest frame ε' as [1]:

$$\varepsilon = \frac{1}{2} m\boldsymbol{v}\cdot\boldsymbol{v} = \varepsilon' + t_p + 2\sqrt{\varepsilon' t_p}\cos\theta', \tag{1a}$$

or its more accurate relativistic counterpart

$$\varepsilon = \gamma_p\varepsilon' + t_p + \sqrt{(1+\gamma')(1+\gamma_p)\varepsilon' t_p}\cos\theta'. \tag{1b}$$

Here, $t_p = (m/M_p)E_p$ is the reduced projectile energy (the kinetic energy of an isotachic electron, also known as the Cusp energy), E_p and M_p are the kinetic energy and mass of the projectile, respectively, while m is the electron mass and $\gamma_p(= 1 + t_p/(mc^2))$ and $\gamma'(= 1 + \varepsilon'/(mc^2))$ are the usual relativistic γ-parameters. Both the second and the third term in Eqs. (1a) and (1b) imply a substantial energy shift from the rest frame energy (the Auger electron energy) ε' to either higher or lower laboratory energies ε depending on the value of θ'. This latter angle determines whether the resulting laboratory electron speed v is larger or smaller than the speed of the electron v$'$ in the projectile rest frame. The third term in Eqs. (1a) and (1b) introduces a stretching effect of the spectra that can be used experimentally with the advantage of achieving high energy resolution measurements. In addition, for fast emitters, there is a limiting laboratory observation angle θ_{max}, as per Fig. 1 [left], beyond which no projectile electrons can be observed. Finally, the relativistic effects at a few MeV/u beam energies are just a small, but observable correction (a few hundred meV) to the measured laboratory electron energy ε. This helps in the more accurate energy calibration and identification of the Auger lines.

For an electron spectrometer with a finite acceptance angle $\Delta\theta'$ (with $\Delta\theta$ in the lab frame), it is simple to show [1], by direct differentiation of Eq. (1) with respect to θ', that the following proportionality holds true:

$$\frac{d\varepsilon}{d\theta'} \propto \sin\theta'. \tag{2}$$

Such a dependence on the finite acceptance angle of the spectrometer induces a kinematic broadening, which is a substantial limiting factor at non-zero observation angles. However, at the observation angle $\theta = 0°$, corresponding to $\theta' = 0°$ or 180°, it follows that $d\varepsilon/d\theta'$ is zero. The implication is that only the second order contributions in $\Delta\theta'$ or smaller are expected. A simple calculation shows that for a practical electron spectrometer acceptance angle of $\Delta\theta \simeq 0.57°$ or $\simeq 10$ mrad, a substantial, almost two-orders of magnitude improvement becomes attainable. This enables high resolution ($\Delta\varepsilon \simeq 100$ meV) electron spectra measurements at realistic count rates. At

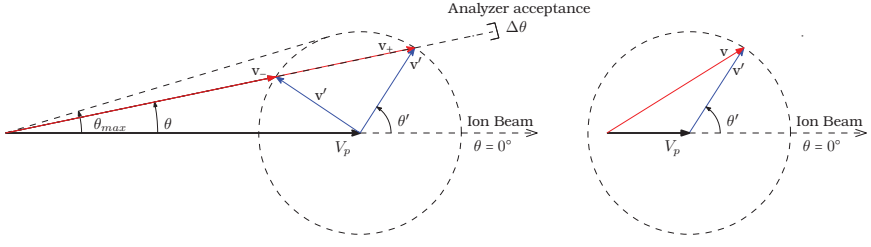

Fig. 1. Velocity addition diagrams. The electron velocity $\boldsymbol{v}'$ in the projectile rest frame is transformed to that in the laboratory frame according to the vector addition rule $\boldsymbol{v} = \boldsymbol{V}_p + \boldsymbol{v}'$, where $\boldsymbol{V}_p$ is the velocity of the projectile emitter. Left: $V_p > v'$ leading to a maximum possible laboratory emission angle θ_{max}. Right: $V_p < v'$, with all observation angles θ being possible. The ZAPS technique sets the electron analyzer at $\theta = 0°$, where kinematic broadening effects due to the finite analyzer acceptance angle $\Delta\theta$ are minimized (see the main text).

$\theta = 0°$, the angle θ' can be either 0° or 180°, according to Fig. 1. This results in a corresponding addition or subtraction of velocities. In such a case, the ensuing laboratory electron energy can be readily obtained from Eq. (1) by setting $\theta' = 0°$ or 180° to be:

$$\varepsilon_{\pm}(\theta = 0°) = (\sqrt{\varepsilon'} \pm \sqrt{t_p})^2, \tag{3a}$$

or its more accurate relativistic counterpart

$$\varepsilon_{\pm}(\theta = 0°) = \frac{1}{2}\left[\sqrt{(1+\gamma_p)\varepsilon'} \pm \sqrt{(1+\gamma')t_p}\right]^2. \tag{3b}$$

In Fig. 2, we show typical high resolution zero-degree electron spectra, where the + sign in Eq. (3) is applicable. The projectile lines corresponding to KLL-Auger transitions are well resolved. The particular states can be readily identified by comparison to the available atomic structure calculations [12].

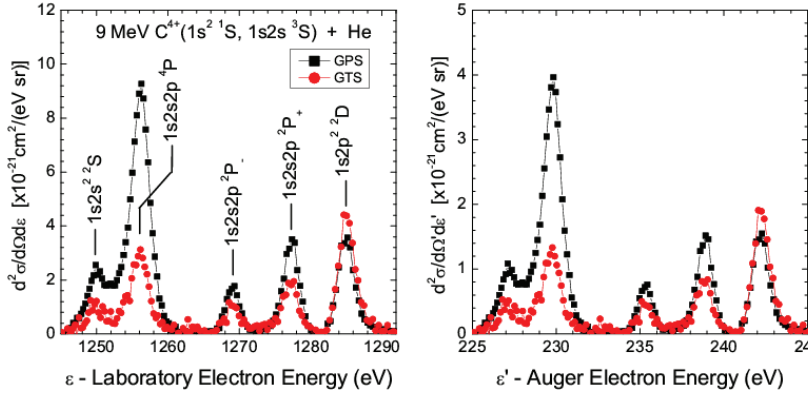

Fig. 2. Typical ZAPS electron spectra obtained with our new apparatus at Demokritos for 9 MeV C^{4+} collisions with helium gas. Left: Laboratory frame spectra. Right: The corresponding projectile rest frame spectra. The spectra were obtained by: Gas Post-Stripping (GPS) the delivered C^{3+} beam to the final C^{4+} beam (squares), Gas Terminal Stripping (GTS) of the C^{-} beam in the terminal of the accelerator (circles). As can be seen, these different stripping methods produce different ratios of the $^4P/^2D$ line intensities. This implies different amounts of pre-excited metastable fraction $1s2s\,^3S$. The energy axes are related by Eq. (1), while the axes of double differential cross sections have been transformed according to Eq. (4).

In addition to the transformation of the energy axis, there is also a corresponding transformation of the double differential cross section (DDCS) on the y-axis such that:

$$\frac{d^2\sigma}{d\Omega' d\varepsilon'} = \sqrt{\frac{\varepsilon'}{\varepsilon}}\,\frac{d^2\sigma}{d\Omega d\varepsilon}. \tag{4}$$

In the case of Fig. 2, since $\varepsilon' < \varepsilon$, the transformation of Eq. (4) to the rest frame shows that the spectra in the laboratory frame are relatively enhanced by the factor $\sqrt{\varepsilon/\varepsilon'}$, which is an additional help.

As illustrated in Fig. 1, for fast emitters ($V_p > \mathrm{v}'$ or equivalently $t_p > \varepsilon'$), there can be two possible solutions $\varepsilon_\pm$ (with corresponding velocities $\mathrm{v}_\pm$) for the same laboratory emission angle θ. For slow emitters ($V_p \leq \mathrm{v}'$ or equivalently $t_p \leq \varepsilon'$), there is only one solution. On the other hand, for fast emitters, this results in a restriction on the emission angle θ to within a maximum value:

$$\theta_{max} = \arcsin\left(\frac{\mathrm{v}'}{V_p}\right), \tag{5}$$

or its more accurate relativistic counterpart resulting from Eq. (1b)

$$\theta_{max} = \arcsin\left\{1 + \gamma_p^2\left[\left(V_p/\mathrm{v}'\right)^2 - 1\right]\right\}^{-1/2}. \tag{6}$$

2.2. *The ZAPS experimental setup of the APAPES project*

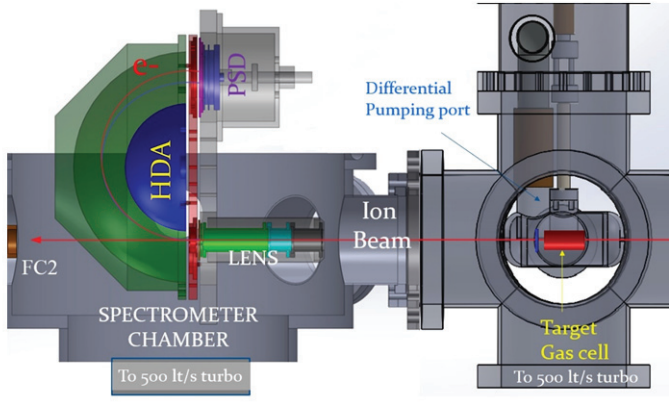

Fig. 3. Our experimental setup consists (from right to left) of a doubly differentially pumped target gas cell, a 4-element entry lens, a large HDA with a 40 mm diameter two-dimensional PSD. The length of the target gas cell is $L_c = 50$ mm and the distance of its center to the lens entry is $s_0 = 289$ mm (see also Fig. 8).

The ZAPS experimental setup of the APAPES project is hosted on beam line L45 at the Demokritos TANDEM measurement hall dedicated to atomic collision physics and is shown in Fig. 3. The mixed state C^{4+} ion beam supplied by the TANDEM is directed into a doubly differentially pumped gas cell where it collides with the target gas. With this system, a stable analyzer chamber vacuum of 10^{-6} Torr can be maintained for typical gas cell pressures in the mTorr range. The emitted Auger electrons are analyzed in energy with a maximum resolution $\Delta\varepsilon/\varepsilon \simeq 0.1\%$ using an electrostatic paracentric hemispherical deflector analyzer (HDA) [13–17] equipped with a 4-element focusing/deceleration entry lens and a two-dimensional (2D) position sensitive detector (PSD) [18, 19]. Since the energy resolution is fixed by the spatial characteristics of the analyzer, higher absolute resolution $\Delta\varepsilon$ is achieved by pre-retarding the Auger electrons. A pre-retardation factor of $F = 4$ is usually sufficient to resolve the Li-like KLL-Auger lines presented here. Finally, the analyzed electron spectra are normalized to the number of ions collected in the final Faraday Cup (FC2) located at the

exit after the HDA (see Fig. 3).

The most critical part of the spectrometer is the four-element electrostatic lens which focuses the emitted electrons from the gas cell to the entry of the HDA. This provides a much smaller virtual slit of less than a millimeter compared to the much larger (6 mm) diameter of the physical HDA entry aperture. Such an arrangement has been found very successful [18] since it allows for the unobstructed passage of the ion beam through the entire lens and the HDA without the production of spurious background electrons. At the same time, it provides the appropriate conditions for high transmission and high energy resolution electron optics in the combined lens plus HDA system. Thus, a single-stage arrangement can be used, as opposed to the conventional two-stage arrangement. This facilitates the use of a 2D PSD instead of the conventional slit exit to increase the overall counting efficiency by at least two orders [20]. The entire system has been simulated [21] in detail (see Fig. 4) by the ion and electron optics simulator – SIMION [22], which provides an alternative, well-tested [15] way to determine the appropriate voltages on both lens and the HDA for optimal operation. The resulting full width at half maximum (FWHM) energy resolution as a function of the pre-retardation parameter F is shown in Fig. 5.

Following the successful installation and testing both the terminal gas stripper and foil/gas post-strippers, we have been able to obtain Auger spectra with variable amounts of metastable beam fraction as already shown in Fig. 2. We then apply the new technique recently developed for the accurate determination of the electron capture ratio R_m [23] (see section 4.4 under the technical restrictions of our method).

3. Ion beam stripping considerations — production of pre-excited ions

The number of electrons carried into the collision by the projectile is important since it also determines the resulting atomic state after the collision, depending on whether a net ionization, excitation or capture process takes place. Highly-charged ions typically carry just a few electrons, resulting in easier interpretable collision spectra which, in turn, can provide more stringent tests of theory [1].

The production of highly-charged ions is, therefore, of great interest in ion-atom collisions. Such ions are typically produced by passing a low charge state beam through a thin foil or gas, where numerous electrons can

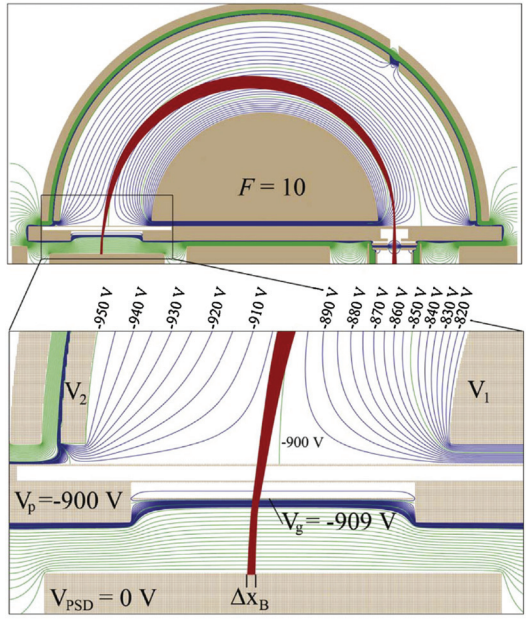

Fig. 4. Details of SIMION schematic of the HDA electrodes, equipotentials and trajectories in the symmetry plane $y = 0$. The insert shows the PSD region at the exit of the HDA for pre-retardation factor $F = 10$ (adapted from Ref. [21]).

be stripped from the ion, thus increasing its charge state. These strippers are found in the terminal of all tandem Van de Graaff accelerators since they are needed to convert the initially negatively charged ion beam to a subsequently positively charged beam, which is further energy boosted in the second stage of acceleration. The desired charge state and energy are typically selected by the analyzing magnet and sent on to the experiment. Depending on the energy of the ion beam during the stripping process, a particular Gaussian-like charge state distribution emerges as being centered around the mean charge state. The higher the energy of the beam, the higher the mean charge state [24–26]. Thus, to produce more intense few-electron or even bare ion beams, additional stripping points are provided after the beam exits the accelerator. These are known as post-strippers.

Few-electron ionic beams, depending on the number of electrons, can be delivered in mixed states including ground state and other long-lived metastable components. The lifetimes of the He-like beam metastable components $1s2s\,^3S$ and $1s2s\,^1S$ have been mostly calculated and are seen in

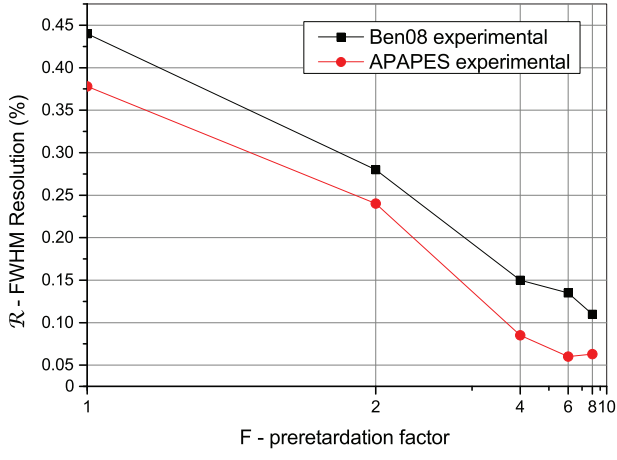

Fig. 5. The FWHM energy resolution is plotted as a function of $1/F$ for preretardation factor F. The FWHM from the older work [15] (squares). The improved FWHM obtained by lens voltages optimized by SIMION [21] (Circles).

Fig. 6(a) to drop rapidly with projectile atomic number Z_p. Assuming the states are statistically produced in a 3 : 1 ratio with a 30% content of $1s2s\,^3S$ at the point of production, we show in Fig. 6(b) the surviving fraction from either the terminal stripper in the accelerator tank (at a distance s_1 = 25.4 m) or the post-stripper (at a distance s_2 = 10 m), away from the target interaction region of our experiment, as a function of Z_p. Clearly, because of its much longer lifetime, the $1s2s\,^3S$ fraction remains practically intact over the whole range of Z_p = 3 – 9, while the $1s2s\,^1S$ fraction is considerably reduced (in the present case of the C^{4+} beams) to below 5%. Therefore, the $1s2s\,^1S$ fraction has been assumed to have a negligible effect on the analysis.

An additional requirement of the APAPES project is to also have a variable (and controllable) amount of metastable beam component ($1s2s\,^3S$). To date, there are no codes that can generally predict the fraction of metastable ions. However, previous studies have shown that the amount of metastable beam components varies mainly depending on whether a foil or a gas stripper is used. The metastable amount of $1s2s\,^3S$ typically reaches a maximum of ~30% for He-like ions, when using a foil stripper [28–33]. We have recently installed a gas terminal stripper inside the TANDEM which produces the He-like beam predominantly in the ground state. By performing two different measurements with beams of appreciably different

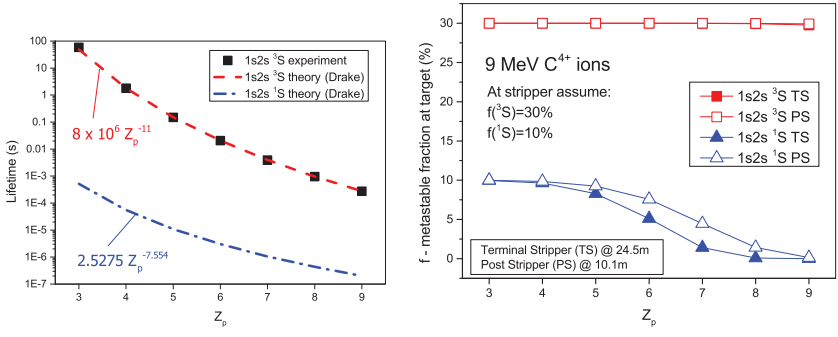

(a) Lifetimes of states. (b) Survival of metastable fractions.

Fig. 6. Parameters of the $1s2s\,^3S$ and $1s2s\,^1S$ levels as a function of projectile atomic number Z_p. (a) Lifetimes calculated by Drake [27]. The explicit Z_p dependencies are the results of least square fits (this work). (b) Survival of metastable fractions from their point of production either at the TANDEM tank terminal stripper or at the post-stripper (see the main text). The two square symbols overlap.

metastable fractions [33, 34], we can extract the contributions from either the ground state or the metastable state. This technique has been presented in detail in a recent publication [23].

4. Single-electron capture

In ion-atom collisions one of the more interesting processes that can be investigated is electron capture to excited atomic states. In single electron capture, an electron is transferred from the target atom to the projectile ion. Details of the electron transfer process depend on the collision system investigated. The information about the transfer to excited states of the projectile can be inferred spectroscopically by observing various transitions (either radiative [35, 36] or Auger [37]) from the excited atomic states to lower lying states.

4.1. *Capture to the metastable* $1s2s\,^3S$ *beam component*

Recently, interest has focused on electron capture to pre-excited states of ions [37–41], i.e. to collisions in which the incoming ion is already in some excited state. This allows for the investigation of excited states not readily produced in any other way. Thus, for example, the spectra shown in Fig. 2 were obtained using the two-electron C^{4+} ion beams in a mixture of

pre-excited $1s2s\,^3S$ and $1s^2$ ground states. The $1s2s\,^3S$ state is metastable (long-lived) since it can only decay by a forbidden spin changing transition. The $1s2s\,^3S$ state is produced in the ion stripper inside the tandem accelerator terminal together with the ground state ions in variable amounts 5-30%, depending on the stripping medium (gas or foil) and stripping energy [29, 31]. Capture to the ground state $1s^22s$ of the formed Li-like ion cannot further de-excite so this transition is not accessible spectroscopically. However, electron capture to the $1s2s\,^3S$ metastable state leads to a spectroscopically rich spectrum:

$$C^{4+}(1s2s\,^3S) + e^- \rightarrow C^{3+}[(1s2s\,^3S)n\ell] \qquad (n \geq 2,\ 0 \leq \ell \leq n-1). \tag{7}$$

The excited states formed in the case of $n = 2$ (according to electron spin-orbit coupling rules) are identified in the spectra of Fig. 2 from their characteristic Auger energies ε'_A:

$$\begin{aligned} &C^{3+}[1s2s2\ell\,^{2S+1}L_J] \qquad (L = \ell = 0, 1,\ S = 3/2, 1/2,\ \boldsymbol{J} = \boldsymbol{L} + \boldsymbol{S}) \\ &\qquad\downarrow \\ &C^{4+}(1s^2) + e^-_A(\varepsilon'_A). \end{aligned} \tag{8}$$

Thus, the production of the $1s2s^2\,^2S$ and $1s2s2p\,^{2,4}P$ lines observed in the Auger spectra can be readily produced by direct single $2s$ or $2p$ electron capture into the $1s2s\,^3S$ component of the ion beam [40, 42]. However, the line labeled as $1s2p^2\,^2D$ cannot be produced by single electron capture to the $1s2s\,^3S$ state since it requires an additional $2s \rightarrow 2p$ excitation. In the energy range of these collisions, another related two-electron process involving the transfer of a target electron to the $2p$ orbital simultaneously with $1s \rightarrow 2p$ excitation from the ground state is quite probable. This process, known as transfer-excitation (TE) [43, 44], can populate the other two observed ^2P lines (through a simultaneous $2s$ transfer/$1s \rightarrow 2p$ excitation), but not the ^4P line. This again has to do with active spin selection rules which would require a low probability spin flipping TE transition to occur from the ground state. Therefore, according to our present understanding [23], the ^4P line is produced only from the metastable state by direct single electron capture [40, 42], while the ^2D line stems dominantly from the ground state through the aforementioned TE process.

Finally, the inherent long lifetime (ns-μs depending on projectile atomic number Z_p and total angular momentum J) of the $1s2s2p\,^4P_J$ metastable states (with $J = 1/2, 3/2, 5/2$ lines unresolved) leads to an additional difficulty in the quantitative analysis of the measured $1s2s2p\,^4P$ production

cross section [34, 42]. In zero-degree measurements, the electron spectrometer lies in the direct path of the ion beam. Therefore, the metastable projectile states decay all along the ionic projectile path towards and through the spectrometer. Thus, one has to correctly take into account both the decay of these states along the path of observation and the increase of the spectrometer acceptance solid angle, as the emission point approaches the entry of the spectrometer. This can result in a considerable correction to the measured metastable electron yield. This correction has been treated in the literature, either in a purely geometrical approach [34, 42] or very recently, for our measurements using an HDA with entry lens, in a Monte Carlo (MC) electron trajectory simulation approach within the SIMION [22] charged particle optics software [45]. In this latter approach, kinematic effects, particular to Auger emission from fast moving projectile ions (e.g. kinematic line broadening and solid angle limitations due to θ_{max}) are included for the first time. This allows for a more accurate and realistic line shape modeling [45] of both metastable and prompt (much shorter lifetimes less than a few ps) Auger lines. The APAPES project has embarked on an isoelectronic study of electron transfer to the $1s2s\,^3S$ state of He-like ions to shed more light on these processes.

4.2. *Separation of contributions from the $1s^2$ ground state and the $1s2s\,^3S$ metastable state component*

The processes that predominantly contribute to the production of the five KLL states of interest are shown in Fig. 7. In general, we may write for the single differential yield of each level x (for $x: {}^2S, {}^2P_\pm, {}^4P, {}^2D$):

$$\frac{dY[x]}{d\Omega'} = (1 - f_{^3S})\left(\frac{d\sigma_g[x]}{d\Omega'}\right) + f_{^3S}\left(\frac{d\sigma_m[x]}{d\Omega'}\right), \tag{9}$$

where $d\sigma_g[x]/d\Omega'$ and $d\sigma_m[x]/d\Omega'$ represent the differential production cross sections for all possible processes that can populate the state x from either the ground state (g) or metastable states (m). The single differential yield is the yield normalized to the total number of ions in the beam N_I (no matter with which beam components these ions are associated):

$$\frac{dY}{d\Omega'}[x] = \frac{N^e[x]}{\kappa\, G_\tau[x]\, \xi[x]}. \tag{10}$$

Here, $\xi[x]$ is the Auger yield and $N^e[x]$ is the total number of electrons in the Auger peak x divided by the overall absolute "normalization" constant

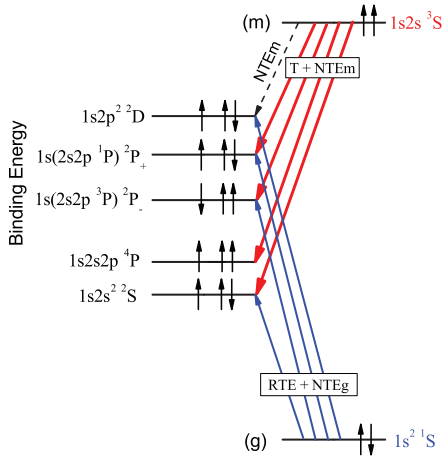

Fig. 7. Energy level diagram showing the dominant mechanisms for the production of the $1s2l2l'\,^{(2S+1)}L$ doubly excited states formed in collisions of energetic He-like ($1s^2\,^1S, 1s2s\,^3S$) beams with low Z_t targets (e.g. H_2). Single $2p$ or $2s$ electron transfer (ET) or non-resonant transfer excitation (NTEm) to the metastable state (m), simultaneous transfer and excitation [both resonant (RTE) and non-resonant (NTEg)] from the ground state (g) (for more details, see the main text).

κ for each Auger line given by:

$$N^e[x] \equiv \int_{[x]} N^e(\varepsilon')\frac{d\varepsilon'}{\Delta\varepsilon} = \int_{[x]} \left(\frac{\varepsilon'}{\varepsilon}\right) N^e(\varepsilon)\frac{d\varepsilon}{\Delta\varepsilon}, \tag{11}$$

$$\kappa \equiv N_I\, n\, L_c\, T\, \overline{\eta}\, \overline{\Delta\Omega_0}, \tag{12}$$

$$\overline{\Delta\Omega}[x] = G_\tau[x]\, \overline{\Delta\Omega_0}, \tag{13}$$

where $\overline{\eta}$ is the detection efficiency averaged over the PSD spectrum energy range. Quantity $\overline{\Delta\Omega}[x]$ is the effective solid angle of the measurement, while G_τ is a spectrometer-dependent solid angle correction factor accounting for a possible dependence on the lifetime $\tau[x]$ of the particular state x (more correctly on the product $V_p\tau[x]$, see Refs. [46, 47]). Recall that the doublet states are all prompt, so that $G_\tau \simeq 1$, implying practically the same solid angle $\overline{\Delta\Omega_0}$. On the other hand, the ^4P state is metastable for which $G_\tau \equiv G_\tau[^4P]$ is significantly different from 1. We have recently computed G_τ for the HDA used in this work [45]. Computations of this correction factor for the two-stage parallel plate analyzer (tandem analyzer) have also been reported in Refs. [1, 34, 43, 48]. The exact value of G_τ is an important correction when measuring the Auger electron yield from the ^4P state for

ions with low Z_p. This is further discussed below. Finally, κ is seen to include the values of all the experimental parameters of the measurement and the accuracy of each of these parameters determines the overall systematic uncertainty of the cross section. All the experimental parameters except for G_τ have been collected together into the overall absolute normalization parameter κ, which for our HDA has been computed and shown to have an overall systematic uncertainty $(\Delta\kappa)/\kappa \lesssim 0.17$ [49].

Let us now assume, by reference to Fig. 7, that the ^2S and $^2P_\pm$ levels are populated from both the ground state (g) and the metastable (m) state. Further, let the ^4P level be populated only from the metastable state (by capture). Moreover, let the ^2D level stem from the ground state alone (by TE). Then, it can be shown [23] that the production cross sections for the five levels can be obtained from the single differential yields dY_i (short notation for $dY_i/d\Omega'$) in two measurements having different metastable fractions. These cross sections are given by the following equations:

$$\frac{d\sigma_m[x]}{d\Omega'} = \frac{dY_2[x]\,dY_1[^2D] - dY_1[x]\,dY_2[^2D]}{dY_1[^2D] - dY_2[^2D]}, \tag{14}$$

$$\frac{d\sigma_g[x]}{d\Omega'} = \frac{dY_2[x]\,dY_1[^4P] - dY_1[x]\,dY_2[^4P]}{dY_1[^4P] - dY_2[^4P]}. \tag{15}$$

Note that Eqs. (14-15) satisfy the main assumption $d\sigma_g[^4P]/d\Omega' = d\sigma_m[^2D]/d\Omega' = 0$.

4.3. *Correction for the long lifetime of the* $1s2s2p\,^4P$ *state - the solid angle correction factor* G_τ

The effective solid angle for electrons emitted from some long-lived Auger projectile states, $\overline{\Delta\Omega}$, can be determined adopting the geometry of Fig. 8. A projectile ion beam of velocity V_p is moving along the $+z$ axis and collides with a gas cell target of length L_c, the center of which is at a distance s_0 from the entry opening of the spectrometer. The projectile is collisionally excited to a long-lived J-state, having a lifetime τ_J, and subsequently Auger decays along the path to and through the spectrometer.

Then, the effective solid angle averaged over the length of the gas cell, $\overline{\Delta\Omega_J}$, can be determined from pure geometrical considerations using the double integral:

$$\overline{\Delta\Omega_J}(L, V_p\tau_J, L_c) \equiv \frac{1}{L_c}\int_{z'=0}^{L_c} dz' \int_{z=0}^{L-z'} dz\, \frac{e^{-z/V_p\tau_J}}{V_p\tau_J}\,\Delta\Omega_0(L-z'-z), \tag{16}$$

where L is the maximal distance along the ion trajectory over which significant contributions to the Auger electron line profile can be made [45]. The

solid angle $\Delta\Omega_0(s)$ corresponds to point source emission from a distance s away from the spectrometer entry. For the HDA under study, the solid angle $\Delta\Omega_0(s)$ for point source emission (subtended by the lens entry aperture of radius r at distance s) is given by $\Delta\Omega_0(s) = 2\pi\left(1 - s/\sqrt{r^2+s^2}\right)$.

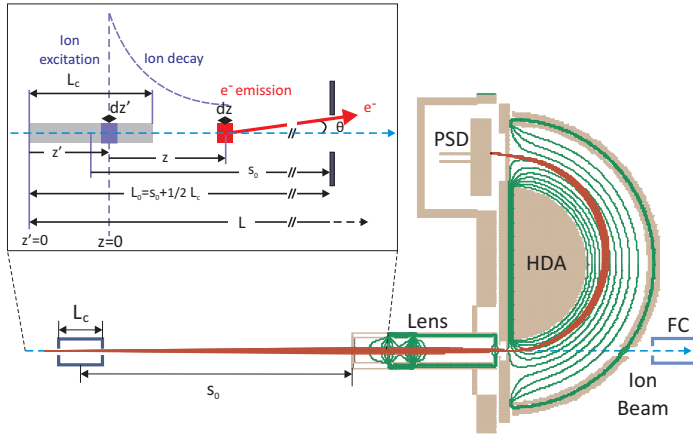

Fig. 8. Schematic geometries for the HDA spectrometer [45]. The ion beam propagates from the gas cell to and through the spectrometer to be finally collected by the FC2. Electron trajectories emitted at the 0° angle with respect to the ion beam are energy analyzed and detected at the two-dimensional PSD. Equipotential lines are also indicated. The insert shows the parameters relevant to the integrations of Eq. (16). Their values are: L_c = 50 mm, r = 2 mm and s_0 = 289 mm [21].

Regarding Eq. (16), it becomes clear that $\overline{\Delta\Omega_J}$ accounts for two competing effects: (i) the gain in the solid angle as the ions approach the spectrometer and (ii) the loss due to the temporal decay along the ion path towards and beyond the spectrometer. A more detailed examination of these effects is given in Ref. [45].

Applying Eq. (16) to a prompt state in the limit of $V_p\tau_J \to 0$, the effective solid angle becomes:

$$\overline{\Delta\Omega_0}(s_0, L_c) \equiv \frac{1}{L_c}\int_{z'=0}^{L_c} dz' \Delta\Omega_0(L_c/2 + s_0 - z'). \tag{17}$$

Thus, we can define the effective solid angle correction factor for the J-state as the ratio of the effective solid angle of the long-lived state to that of the same, but for prompt emission, i.e.:

$$G_{\tau_J} = G_{\tau_J}(L, V_p\tau_J, s_0, L_c) \equiv \frac{\overline{\Delta\Omega_J}(L, V_p\tau_J, L_c)}{\overline{\Delta\Omega_0}(s_0, L_c)}. \tag{18}$$

To account for the J sub-levels, since they are not energy resolved experimentally, a statistical averaging over all the J-states leads to the J-averaged effective solid angle correction factor G_τ given by [45]:

$$G_\tau = \frac{\sum_J (2J+1)\xi_J G_{\tau_J}(L, V_p\tau_J, s_0, L_c)}{\sum_J (2J+1)\xi_J}. \tag{19}$$

4.3.1. *Determination of G_τ: SIMION simulations*

In Ref. [45], we evaluated G_τ for our HDA using MC-type simulations realized within the SIMION 8.1 ion optics package in the following way. For a number N_0 of initially (t=0) populated projectiles for each J-state, the number of the observed Auger electrons will be:

$$N^e_{obs_J} \sim \xi_J N_0 \overline{\Delta\Omega_J}(L, V_p\tau_J, L_c). \tag{20}$$

However, the true number of detected electrons should be:

$$N^e_{true_J} \sim \xi_J N_0 \overline{\Delta\Omega_0}(s_0, L_c), \tag{21}$$

so that

$$\frac{N^e_{obs_J}}{N^e_{true_J}} = \frac{\overline{\Delta\Omega_J}(L, V_p\tau_J, L_c)}{\overline{\Delta\Omega_0}(s_0, L_c)} \equiv G_{\tau_J}. \tag{22}$$

Therefore, the ratio of the number of observed electrons of a long-lived J-state to the number of true electrons, which corresponds to a prompt state of the same initial population N_0, essentially describes the effective solid angle correction factor G_{τ_J}. The J-averaged effective solid angle correction factor G_τ is then estimated through Eq. (19).

4.3.2. *Experimental determination of G_τ using Be-like carbon beams*

The experimental determination of G_τ was based on the fact that the Be-like ions produced in tandem Van de Graaff accelerators are delivered in mixed ionic states, including the ground $1s^2 2s^2\ {}^1S$ and the metastable $1s^2 2s2p\,{}^3P_J$ states with lifetimes in the μs-to-s range (depending again on atomic number Z_p and angular momentum J) [50–52]. In collisions with the H_2 targets, the $1s$ electron of the $1s^2 2s2p\,{}^3P$ state is needle ionized [53] (similar to the situation encountered in photo-ionization of Be-like ions [52, 54–57]). This results in the production of the $1s2s2p$ configuration, which in the LS coupling scheme gives rise to the $1s2s2p\,{}^4P$ and $1s(2s2p\,{}^3P)^2P$ states (or ${}^2P_-$ for short). These two states are used in our

experimental determination of the effective solid angle correction factor G_τ. As already mentioned, the ^4P state is a long-lived state which Auger decays to the $1s^2$ ground state. On the other hand, the $^2P_-$ state Auger decays promptly to the $1s^2$ ground state having lifetimes ranging from tens to hundreds of fs.

In addition, the production population statistics of the ^4P and $^2P_-$ states should result in the ratios $\sigma(^4P) : \sigma(^2P_-) = 2 : 1$, as follows from the multiplicity of the states. A direct measurement of this ratio requires the necessary correction due to the metastability of the ^4P state and, therefore, the determination of the effective solid angle correction factor G_τ. Thus, we have:

$$\frac{\sigma(^4P)}{\sigma(^2P_-)} = \frac{Y(^4P)/(\xi_{^4P}G_\tau)}{Y(^2P_-)/\xi_{^2P_-}} = 2, \tag{23}$$

and, therefore,

$$G_\tau = \frac{1}{2}\frac{Y(^4P)}{Y(^2P_-)}\frac{\xi_{^2P_-}}{\xi_{^4P}}, \tag{24}$$

where Y denotes the measured normalized electron yields obtained from the fitted areas, while the values of the Auger yields are adopted from Ref. [58].

The production of the ^4P and $^2P_-$ states, by $1s$ ionization of the $1s^2 2s2p\,^3P$ beam component has an advantage crucial to the correct determination of the G_τ correction factor: it is free from additional deleterious effects on their ratio which can modify its spin statistics value of 2. As mentioned earlier, the ^4P and $^2P_-$ states can also be populated in collisions of He-like ions delivered in mixed $(1s^2, 1s2s\ ^3S)$ states via single capture to the $2p$ state. However, capture to higher $n\ell$-states is known to be strong [41, 59] and, as such, can lead to cascade feeding of these states [60], which could alter their expected spin statistics population ratio [61].

In Fig. 9, we present high resolution electron spectra measured with our HDA in 17.5 MeV collisions of O^{4+} with H_2. The electrons were recorded at pre-retardation factor F=8 for higher resolution. As can be seen, the small asymmetry in the peak near 425 eV is due to the additional low intensity $1s2s^2 2p\,^3P$ Auger line, which was also reported for similar spectra in Ref. [62]. This state can be formed from the $1s^2 2s^2\ ^1S$ ground state via $1s \rightarrow 2p$ excitation, and it will promptly decay to the $1s^2 2p$ final state. It is important to account for this extra peak area for the accurate determination of G_τ. Therefore, the line spectra were fitted with the Voigt profiles, except for the ^4P peak whose asymmetric profile, due to its metastability, was considered in the fitting process. The $1s2s^2 2p\,^3P$ peak area was found to be about 17% of the total area of both peaks in the vicinity of 425 eV.

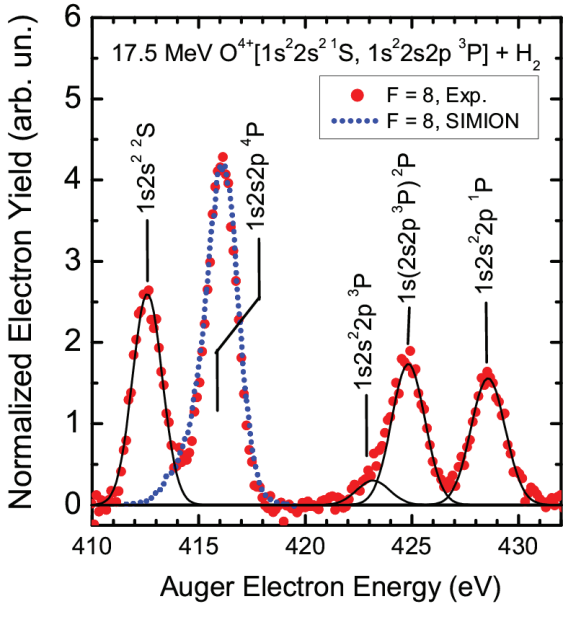

Fig. 9. Oxygen Auger KLL spectra obtained in collisions of 17.5 MeV O^{4+} with H_2 using our HDA spectrometer. The SIMION simulations of the ^4P spectral distributions are shown by the dotted lines in excellent agreement with the measurements. The solid lines correspond to the Voigt profile least square fits of the peaks. The small peak at the low energy shoulder of the $1s(2s2p^3P)\ ^2P$ peak, was identified as arising from the $1s2s^22p\ ^3P$ intermediate state [62]. Its contribution was carefully accounted for and separated from that of the $^2P_-$ peak of primary interest (see the main text).

Our results for the collision system O^{4+} + H_2 at 17.5 MeV with two different deceleration factors (F = 4 and F = 8), as well as for the collision system C^{2+} + H_2 at 6.6 MeV with the deceleration factor of F = 4 are presented in Table 1.

For the case of oxygen, the G_τ values obtained with SIMION are comparable to the estimated experimental uncertainty of the measured values, for the lifetimes reported in Ref. [63], while they deviate by an additional ~ 20% for the lifetimes reported in Ref. [58]. However, in the case of carbon, the SIMION results are well within the experimental uncertainties. Further, it is seen from Table 1, that G_τ depends sensitively on the lifetimes and the involved Auger yields, as evident from the ≃ 15% differences in the estimated values of G_τ using the lifetimes reported in Refs. [46] and [58],

Table 1. Results for the effective solid angle correction factor G_τ determined experimentally (denoted as "Exp.", referred to Eq. (24)) and by the MC-type SIMION simulations.

State	E_p MeV	F	G_τ Exp.	G_τ SIMION
C^{2+}	6.6	4	2.0(4)	1.92[a]
				2.41[b]
O^{4+}	17.5	4	1.9(4)	2.47[a]
				2.80[b]
		8	1.5(4)	2.08[a]
				2.33[b]

[a] See Ref. [46], [b] see Ref. [58].

both for oxygen and carbon. Clearly, this sensitivity on the lifetimes can be a source of considerable systematic theoretical uncertainty in the estimation of G_τ. Thus, overall, we may claim that an acceptable agreement was found between our SIMION computations and the measured values of G_τ.

4.4. *Capture to metastable ratios R_m and r_m*

Basic quantum mechanics requires the spin coupling of the $2p$ electron to the $1s2s\,^3S$ state yielding $1s2s2p\,^4P$ quartet and $1s2s2p\,^2P$ doublet states to be in the ratio of $2:1$, i.e.:

$$R_m \equiv \frac{\frac{d\sigma_m[^4P]}{d\Omega'}}{\frac{d\sigma_m[^2P_+]}{d\Omega'} + \frac{d\sigma_m[^2P_-]}{d\Omega'}}, \tag{25}$$

while the ratio r_m

$$r_m \equiv \frac{\frac{d\sigma_m[^2P_+]}{d\Omega'}}{\frac{d\sigma_m[^2P_-]}{d\Omega'}}, \tag{26}$$

should be equal to 3. Here, σ_m is the capture cross section into the particular state [63]. Thus, it came as a big surprise that the measured ratio R_m was found to significantly deviate for the C^{4+} beams [40], clearly calling for an explanation. A new two-electron process termed the Pauli exchange interaction was subsequently proposed [40], where a target electron, which is spin-aligned with the two projectile electrons in the $1s2s\,^3S$ state, experiences a (slightly) different potential than an anti-aligned electron. If the interaction potentials are different, the outcomes (^4P vs. ^2P formation) could also be different. This process does not necessarily involve excitation

of the projectile $1s$ electron and could possibly be described within the independent electron model, but one would need spin-dependent potentials - a difficult task - not yet attempted [64].

However, more recently, it has been shown that capture to higher-lying ($1s2lnl'\,^{2,4}L_J$) states with $n > 2$ should also be very probable. Therefore, selective cascade feeding of the $1s2s2p\,^4P$ can also be expected to occur [34, 41, 60]. All the higher-lying doublet states Auger decay strongly to the K-shell, while the higher-lying quartet Auger decay much more weakly due to spin selection rules. The $E1$ transition rates, however, are the strongest for quartet to quartet and/or doublet to doublet transitions. This results in a selective cascade feeding mechanism directly enhancing just the ^4P populations.

Utilizing our method, presented in Sec. 4.2, for separating the contributions for the $1s2s\,^3S$ metastable and the $1s^2\,^1S$ ground states, the ratio R_m can be directly obtained in terms of the measured parameters using Eqs. (14) and (15):

$$R_{m,exp} = \frac{\frac{1}{G_\tau\,\xi[^4P]}\left(\frac{dY_2[^4P]}{dY_2[^2D]} - \frac{dY_1[^4P]}{dY_1[^2D]}\right)}{\frac{1}{\xi[^2P_+]}\left(\frac{dY_2[^2P_+]}{dY_2[^2D]} - \frac{dY_1[^2P_+]}{dY_1[^2D]}\right) + \frac{1}{\xi[^2P_-]}\left(\frac{dY_2[^2P_-]}{dY_2[^2D]} - \frac{dY_1[^2P_-]}{dY_1[^2D]}\right)}. \qquad (27)$$

As can be seen, R_m is expressed as the ratios of the peak areas of the same spectrum (the same measurement) in which the absolute normalization parameters κ have canceled, while there is no direct evidence of the metastable fractions. Clearly, this is a considerable advantage since both the absolute normalization and metastable fraction determination are generally more tedious to obtain because special attention is required regarding some additional experimental details. Thus, except for the theoretically determined P state the Auger yields $\xi[^2P_\pm]$ appearing in all the ratios, only the solid angle correction factor G_τ and the Auger yield $\xi[^4P]$ are needed for $R_{m,exp}$. Moreover, since the angular distributions of the Auger decays from the ^4P and ^2P states can be expected to be quite similar (both are the P states), it follows that $R_{m,exp}$ practically corresponds to the ratio $\sigma_m[^4P]/\sigma_m[^2P]$ of the total production cross sections.

In Fig. 10a, we present various results for R_m from the literature as well as from our recent measurements for collisions with helium targets. It is clearly seen that the results for B^{3+}+H_2 (filled rectangles), F^{7+}+H_2 (filled triangles), as well as for our recent C^{4+}+He work (filled circles) show R_m to be close to the statistically expected value of two. This is much better than the originally reported measurements of Strohschein *et al.* [34] (open

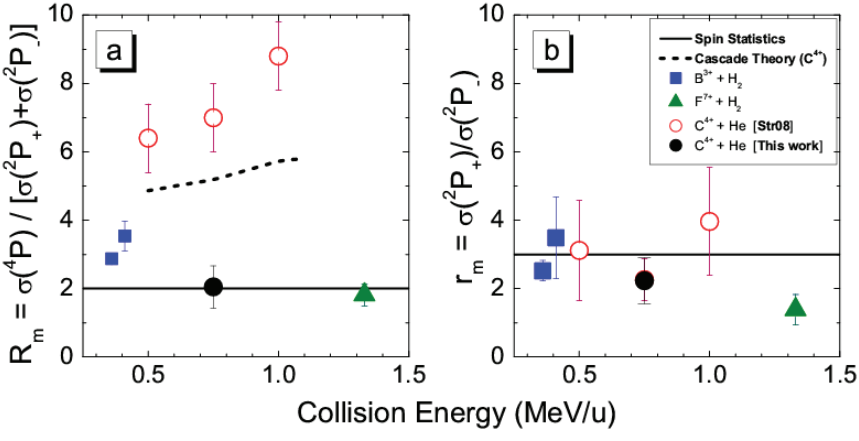

Fig. 10. Determination of the ratios R_m [a] and r_m [b] as a function of collision energy. Symbols: Experimental results. Lines: Theory. Filled rectangles: B^{3+}+H_2, filled triangles: F^{7+}+H_2 (reported by Benis *et al.* [63] from our older work). Open circles: C^{4+}+He (R_m from Strohschein *et al.* [34], with r_m values extracted from the same data and reported in Ref. [63]). Filled circles: C^{4+}+He (present). Dashed line: Theory including cascade feeding for $n \rightarrow \infty$+ Auger (Röhrbein *et al.* [60]).

circles) giving the values of R_m as large as 9. In Fig. 10b, we also include the results from the recent computation [63] of the ratio r_m via Eq. (26). This ratio, according to theory, is expected to be equal to 3 and, moreover, it should be independent of the solid angle correction factor G_τ. In this case, practically all the measurements, including those with very different R_m, are in much better agreement with theory. This, therefore, casts some doubt on the G_τ correction factors used by Strohschein *et al.* [34] which, in fact, were found recently [47] to be incorrectly computed.

In the context of this sub-section, it is pertinent to recall Fig. 2, where we display our recently obtained KLL spectra at 9 MeV for C^{4+}+He from two measurements having quite different metastable fractions. The high value metastable fraction was obtained after gas post-stripping the C^{3+} beam in the N_2 gas. The low value fraction was obtained by stripping the initial C^- beam in the N_2 gas inside the terminal of the tandem accelerator. The increased metastable fraction was readily manifested in the KLL spectra of Fig. 2 by the enhanced production of the ^4P state (squares) as opposed to the smaller production at the lower fraction (circles).

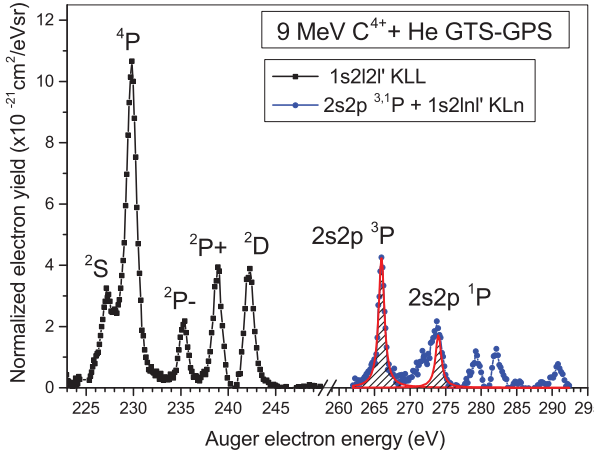

Fig. 11. The 9 MeV $C^{4+}(1s^2, 1s2s\,^3S)$ collisions with He. Auger lines: $C^{3+}(1s2l2l')$ KLL (squares), $C^{4+}(2s2p\,^{3,1}P)$ KLL (circles) and $C^{3+}(1s2s\,^3S)n\ell$ KLn (n = 3 – 4). The $1s \rightarrow 2p$ excitation lines are shown by the fits (shaded areas). The beam was produced by gas stripping in the accelerator terminal, GTS, and subsequent gas post stripping, GPS, of the analyzed C^{3+} ions.

5. $1s - 2p$ excitation of the metastable $1s2s\,^3S$ beam component

To obtain an independent cross-check on the $C^{4+}(1s2s\,^3S)$ metastable beam fraction (apart from the new method recently introduced and based upon the analysis of the Auger KLL lines in He-like beams with different metastable fractions [23]), we have also explored the production of various Auger lines of slightly higher electron energy such as the He-like $2s2p\,^{3,1}P$ KLL produced by $1s \rightarrow 2p$ excitation shown in Fig. 11. These lines are also of particular importance in the detailed study of fundamental mechanisms of excitation [42], i.e. the electron-nucleus, electron-electron and electron-electron excitation with spin exchange [65].

The presently unidentified lines in Fig. 11 are most probably due to $(1s2s\,^3S)n\ell$ Li-like states [66] produced by direct $n\ell$ capture with n = 3 and 4 to the metastable $1s2s\,^3S$ beam component. Their existence would be further proof that these higher lying states are produced by capture as required by the proposed cascade mechanisms leading to the reported enhancement of the ^4P population [34, 41, 60].

6. Summary, conclusions and future directions

We have presented the basics of the ZAPS technique used at the new experimental station dedicated to atomic collisions physics at the Demokritos TANDEM. This apparatus is now in operation and can perform high resolution Auger electron spectroscopy of projectile ions excited during their collision with gas targets which allows for the state selective determination of differential cross sections. Details of the experimental setup were described with particular application to studies of single electron capture to He-like ions in the pre-excited $1s2s\,^3S$ long-lived state. A terminal gas stripper along with both gas and foil post-strippers has also been installed in the TANDEM to provide more intense He-like beams with variable amounts of the $1s2s\,^3S$ beam fraction.

With the above tools, we have explored capture and excitation using the $C^{4+}(1s^2, 1s2s\,^3S)$ mixed state beams in collisions with various targets in the 0.5-1.5 MeV/u collision energy region. Using our new technique, already presented in detail in Ref. [63], whose results are also briefly presented here, we have been able to determine the capture to metastable ratios R_m and r_m, for various collision systems, including our own recent work for 9 MeV C^{4+}+He. Our results are supported by the accurate determination of the effective solid angle G_τ (crucial for the calculation of R_m) which has also been measured experimentally, and found to be in fair agreement with our MC-type SIMION calculations. The reported values of R_m are mostly close to the expected spin statistics value of 2, but in glaring disagreement both with the experimental results on 6-12 MeV C^{4+}+He from Ref. [34] and the theoretical calculations [60]. Theory, however, clearly demonstrates the selective strong cascade feeding of the ^4P state for these collision systems, in support of the proposed cascade enhancement mechanism [41]. In contrast, the newly reported values of r_m are found to be mostly in good agreement with the expected spin statistics value of 3 [61], even for the R_m disagreeing measurements of Ref. [34].

Thus, even though calculations have shown an enhancement of the ^4P state due to selective cascade feeding in both fluorine [41] and carbon [60] collisions with light targets, there is a rather strong disagreement between the calculated and measured values of R_m, especially for carbon in the 9-12 MeV range. It is still not clear why this cascade enhancement is not observable in the reported measurements. This remains a puzzle to be resolved.

It is evident that more results with careful measurements and theoretical calculations, including cascades, for some other low-Z_p He-like ions will be further needed to convincingly establish the existence of cascade feeding of the ^4P state, as well as to answer the question why this cascade feeding is not clearly identifiable in the measurements of R_m, as presented in here.

In the near future, we plan to finish our measurements and analysis of 6-18 MeV C^{4+} ions in collisions with various gas targets, including H_2, Ne and Ar in an effort to investigate all the possible TE contributions from both the ground state and metastable states to the Auger KLL states. Accurate theoretical calculations are also needed, particularly for NTE from the metastable state (never investigated before). In addition, we plan to finish our investigation of the related excitation channel briefly presented here. Again, accurate theoretical calculations are needed here, as well. Clearly, additional theoretical support would be most welcome in future collaborations.

Acknowledgments

During the period (2012-2015) we acknowledge support by the project APAPES co-financed by the European Union (European Social Fund - ESF) and Greek national funds through the Operational Program "Education and Lifelong Learning" of the National Strategic Reference Framework (NSRF) Research Funding Program: THALES. Investing in knowledge society through the European Social Fund, grant number MIS 377289. For the period of (2017-2020), we acknowledge support by the project "CALIBRA/EYIE" (MIS 5002799) which is implemented under the Action "Reinforcement of the Research and Innovation Infrastructures", funded by the Operational Program "Competitiveness, Entrepreneurship and Innovation" (NSRF 2014-2020) and co-financed by Greece and the European Union (European Regional Development Fund).

On a personal level, it is a pleasure to acknowledge the help of various colleagues during the development of the entire experimental program through 2015, including A. Dimitriou, Be. Sulik, I. Valastyan, O. Sise, G. Martinez, as well as the TANDEM accelerator staff of Tassos Lagoyannis, Michalis Axiotis and Miltos Andrianis. In addition, our thanks also extend to the staff of the J.R. Macdonald tandem accelerator laboratory of Kansas State University and in particular to K. Carnes for his invaluable help on the implementation of the recirculating gas terminal stripper and other components of the APAPES beam line optics and also to K. Bahner,

former technical staff of the now defunct EN tandem accelerator in Aarhus Denmark, for his detailed advise on the implementation of the Steinmetz circuitry used to power the recirculating gas turbomolecular pump. We would also like to thank D. Manura of Scientific Instrument Services for his detailed help with SIMION Lua programming. Last, but not least, we thank the then director of the Institute of Nuclear and Particle Physics at Demokritos, S. Harissopulos, for his enthusiastic encouragement and support through out the entire APAPES program period. Finally, TJMZ also acknowledges the support of ELKE travel grant #4669 of the University of Crete that allowed for his participation at the 25th International Symposium on Ion-Atom Collisions held in Palm Cove, Queensland, Australia on July 23-25, 2017.

References

[1] T. J. M. Zouros and D. H. Lee, Zero Degree Auger Electron Spectroscopy of Projectile Ions, in S. M. Shafroth and J. C. Austin (eds.), *Accelerator-Based Atomic Physics Techniques and Applications*, Chap. 13. American Institute of Physics Conference Series, Woodbury, NY, pp. 426-479 (1997).

[2] N. Stolterfoht, R. D. Dubois and R. D. Rivarola, Electron emission in heavy ion-atom collisions, *Springer Series on Atoms and Plasmas*, Berlin (1997).

[3] Dž. Belkić, Review of theories on ionization in fast ion-atom collisions with prospects for applications to hadron therapy, *J. Math. Chem.* **47**, 1366-1419 (2010).

[4] APAPES Atomic Physics with Accelerators: Projectile Electron Spectroscopy, http://apapes.physics.uoc.gr (2015).

[5] S. Hagmann, T. Stöhlker, J. Ullrich, C. Kozhuharov, R. Moshammer, H. Kollmus, R. Mann and M. Nofal, A forward electron spectrometer for the ESR, *Nucl. Instrum. Methods Phys. Res. B* **205**, 207-209 (2003).

[6] W. Mampe, K. Schreckenbach, P. Jeuch, B. Maier, F. Braumandl, J. Larysz and T. von Egidy, The double focusing iron-core electron-spectrometer "*BILL*" for high resolution (n, e^-) measurements at the high flux reactor in Grenoble, *Nucl. Instrum. Methods* **154**, 127-149 (1978).

[7] Y. Litvinov, F. Attallah, K. Beckert, F. Bosch, D. Boutin, M. Falch, B. Franzke, H. Geissel, M. Hausmann, T. Kerscher, O. Klepper, H.-J. Kluge, C. Kozhuharov, K. Löbner, G. Münzenberg, F. Nolden, Y. Novikov, Z. Patyk, T. Radon, C. Scheidenberger, J. Stadlmann, M. Steck, M. Trzhaskovskaya and H. Wollnik, Observation of a dramatic hindrance of the nuclear decay of isomeric states for fully ionized atoms, *Physics Letters B* **573**, Supplement C, 80-85 (2003).

[8] H. Kankaanpää, P. Butlerb, P. Greenlees, J. Bastin, R. Herzberg, R. Humphreys, G. Jones, P. Jones, R. Julin, A. Keenan, H. Kettunen, M. Leino, L. Miettinen, T. Page, P. Rahkila, C. Scholey and J. Uusitalo,

In-beam electron spectrometer used in conjunction with a gas-filled recoil separator, *Nucl. Instrum. Methods Phys. Res. A* **534**, 503-510 (2004).

[9] R. L. Graham, G. T. Ewan and J. S. Geiger, A one-meter-radius iron-free double-focusing $\pi\sqrt{2}$ spectrometer for β-ray spectroscopy with a precision of 1:10^5, *Nucl. Instrum. & Methods* **9**, 245-286 (1960).

[10] K. Schreckenbach, H. Faust, F. V. Feilitzsch, A. Hahn, K. Hawerkamp and J. Vuilleumier, Absolute measurement of the beta spectrum from ^{235}U fission as a basis for reactor antineutrino experiments, *Phys. Lett.* **99B**, 251-256 (1981).

[11] N. Stolterfoht, High resolution Auger spectroscopy in energetic ion atom collisions, *Physics Reports* **146**, 315-424 (1987).

[12] R. Bruch, K. T. Chung, W. L. Luken and J. C. Culberson, Recalibration of the *KLL* Auger spectrum of carbon, *Phys. Rev. A* **31**, 310-315 (1985).

[13] E. P. Benis and T. J. M. Zouros, Improving the energy resolution of a hemispherical spectrograph using a paracentric entry at a non-zero potential, *Nucl. Instrum. Methods Phys. Res. A* **440**, 462-465 (2000).

[14] T. J. M. Zouros and E. P. Benis, Erratum to "The hemispherical deflector analyser revisited. I. Motion in the ideal $1/r$ potential, generalized entry conditions, Kepler orbits and spectrometer basic equation, *J. Electron. Spectrosc. Relat. Phenom.* **125**, 221-248 (2002).", *J. Electron Spectrosc. and Relat. Phenom.* **142**, 175-176 (2005).

[15] E. P. Benis and T. J. M. Zouros, The hemispherical deflector analyser revisited. II. Electron-optical properties, *J. Electron Spectrosc. and Relat. Phenom.* **163**, 28-39 (2008).

[16] O. Sise, M. Ulu, M. Dogan, G. Martinez and T. J. M. Zouros, Fringing field optimization of hemispherical deflector analyzers using BEM and FDM, *J. Electron Spectrosc. and Relat. Phenom.* **177**, 42-51 (2010).

[17] M. Dogan, M. Ulu, G. G. Gennarakis and T. J. M. Zouros, Experimental energy resolution of a paracentric hemispherical deflector analyzer for different entry positions and bias, *Rev. Sci. Instrum.* **84**, 043105 (2013).

[18] E. P. Benis, K. Zaharakis, M. M. Voultsidou, T. J. M. Zouros, M. Stöckli, P. Richard and S. Hagmann, A new hemispherical analyser with 2-D PSD and focusing lens for use in 0° electron spectroscopy, *Nucl. Instrum. Methods Phys. Res. B* **146**, 120-125 (1998).

[19] E. P. Benis, T. J. M. Zouros and P. Richard, High resolution RTE measurements at zero degrees using a Hemispherical analyser with lens and 2-D PSD, *Nucl. Instrum. Methods Phys. Res. B* **154**, 276-280 (1999).

[20] E. P. Benis, T. J. M. Zouros, H. Aliabadi and P. Richard, Hemispherical analyser with 2-D PSD for 0° Auger projectile spectroscopy, *Phys. Scr.* **T80**, 529-531 (1999).

[21] O. Sise, G. Martinez, I. Madesis, A. Laoutaris, A. Dimitriou, M. Fernandez-Martin and T. J. M. Zouros, The voltage optimization of a four-element lens used on a hemispherical spectrograph with virtual entry for highest energy resolution, *J. Electron Spectrosc. and Relat. Phenom.* **211**, 19-31 (2016).

[22] SIMION®Ion and Electron Optics Simulator, *SIS* Scientific Instrument Services, SIMION version 8.1.2.20, Ringoes, NJ, see http://www.simion.com (2014).

[23] E. P. Benis and T. J. M. Zouros, Determination of the $1s2\ell2\ell'$ state production ratios ${}^4P^o/{}^2P$, ${}^2D/{}^2P$ and ${}^2P_+/{}^2P_-$ from fast $(1s^2, 1s2s\,{}^3S)$ mixed-state He-like ion beams in collisions with H_2 targets, *J. Phys. B* **49**, 235202 (2016).

[24] H.-D. Betz, Charge states and charge-changing cross sections of fast Heavy ions penetrating through gaseous and solid media, *Rev. Mod. Phys.* **44**, 465-539 (1972).

[25] R. Sayer, Semi-empirical formulas for heavy-ion stripping data, *Rev. Phys. Appl. (Paris)* **12**, 1543-1546 (1977).

[26] A. Laoutaris, I. Madesis, A. Dimitriou, A. Lagoyannis, M. Axiotis, E. P. Benis and T. J. M. Zouros, Use of gas and foil strippers for the production of He-like ionic beams in both pure ground state $(1s^2)$ and mixed states $(1s^2, 1s2s)$ for zero-degree Auger projectile electron spectroscopy, *J. Phys: Conf. Ser.* **635**, 052062 (2015).

[27] G. W. F. Drake, Theory of relativistic magnetic dipole transitions: Lifetime of the metastable 2 ^{3}S state of the Heliumlike ions, *Phys. Rev. A* **3**, 908-915 (1971).

[28] M. Terasawa, T. J. Gray, S. Hagmann, J. Hall, J. Newcomb, P. Pepmiller and P. Richard, Electron capture by and electron excitation of two-electron fluorine ions incident on helium, *Phys. Rev. A* **27**, 2868-2875 (1983).

[29] M. Zamkov, H. Aliabadi, E. P. Benis, P. Richard, H. Tawara and T. J. M. Zouros, Energy dependence of the metastable fraction in $B^{3+}(1s^2\,{}^1S, 1s2s\,{}^3S)$ beams produced in collisions with thin-foil and gas targets, *Phys. Rev. A* **64**, 052702 (2001).

[30] M. Zamkov, H. Aliabadi, E. P. Benis, P. Richard, H. Tawara and T. J. M. Zouros, Stripping energy dependence of $B^{3+}(1s2s^3S)$ beam metastable fraction, *AIP* **576**, 149-152 (2001).

[31] M. Zamkov, E. P. Benis, P. Richard and T. J. M. Zouros, Fraction of metastable $1s2s\,{}^3S$ ions in fast He-like beams (Z = 5-9) produced in collisions with carbon foils, *Phys. Rev. A* **65**, 062706 (2002).

[32] E. P. Benis, M. Zamkov, P. Richard and T. J. M. Zouros, Techniques for the determination of the $1s2s\,{}^3S$ metastable fraction in two-electron beams, *Phys. Rev. A* **65**, 064701 (2002).

[33] E. P. Benis, M. Zamkov, P. Richard and T. J. M. Zouros, Comparison of two experimental techniques for the determination of the $1s2s^3S$ metastable beam in energetic B^{3+} ions, *Nucl. Instrum. Methods Phys. Res. B* **205**, 517-521 (2003).

[34] D. Strohschein, D. Röhrbein, T. Kirchner, S. Fritzsche, J. Baran and J. A. Tanis, Nonstatistical enhancement of the $1s2s2p\,{}^4P$ state in electron transfer in 0.5-1.0 MeV/u $C^{4,5+}$ + He and Ne collisions, *Phys. Rev. A* **77**, 022706 (2008).

[35] M. Druetta, S. Martin and J. Desesquelles, VUV spectroscopy of charge exchange processes in collisions of multiply charged ions, *Nucl. Instrum. Methods Phys. Res. B* **23**, 268-273 (1987).

[36] S. Bliman, M. Cornille and K. Katsonis, Dielectronic recombination versus charge exchange: Electron capture by metastable ions, *Phys. Rev. A* **50**, 3134-3141 (1994).

[37] E. P. Benis, T. J. M. Zouros, T. W. Gorczyca, M. Zamkov and P. Richard, Isoelectronic study of triply excited Li-like states, *J. Phys. B* **36**, L341-L348 (2003).

[38] M. Zamkov, H. Aliabadi, E. P. Benis, P. Richard, H. Tawara and T. J. M. Zouros, Absolute cross sections and decay rates for the triply excited $B^{2+}(2s2p^2\,{}^2D)$ resonance in electron–metastable-ion collisions, *Phys. Rev. A* **65**, 032705 (2002).

[39] E. P. Benis, T. J. M. Zouros, T. W. Gorczyca, A. D. González and P. Richard, Elastic resonant and non-resonant differential scattering of quasi-free electrons from $B^{4+}(1s)$ and $B^{3+}(1s^2)$ ions, *Phys. Rev. A* **69**, 052718 (2004).

[40] J. A. Tanis, A. L. Landers, D. J. Pole, A. S. Alnaser, S. Hossain and T. Kirchner, Evidence for Pauli exchange leading to excited-state enhancement in electron transfer, *Phys. Rev. Lett.* **92**, 133201 (2004).

[41] T. J. M. Zouros, B. Sulik, L. Gulyas and K. Tokesi, Selective enhancement of $1s2s2p^4P_J$ metastable states populated by cascades in single-electron transfer collisions of $F^{7+}(1s^2/1s2s\,{}^3S)$ ions with He and H_2 targets, *Phys. Rev. A* **77**, 050701 (2008).

[42] D. H. Lee, P. Richard, J. M. Sanders, T. J. M. Zouros, J. L. Shinpaugh and S. L. Varghese, Electron capture and excitation studied by state-resolved *KLL* Auger measurement in 0.25-2 MeV/u $F^{7+}(1s^2\,{}^1S, 1s2s\,{}^3S)$ + H_2/He collisions, *Nucl. Instrum. Methods Phys. Res. B* **56/57**, 99-103 (1991).

[43] D. H. Lee, P. Richard, J. M. Sanders, T. J. M. Zouros, J. L. Shinpaugh and S. L. Varghese, *KLL* resonant transfer and excitation to $F^{6+}(1s2l2l')$ intermediate states, *Phys. Rev. A* **44**, 1636-1643 (1991).

[44] T. J. M. Zouros, Resonant transfer and excitation associated with Auger electron emission, in W. G. Graham, W. Fritsch, Y. Hahn and J. Tanis (eds.), *Recombination of Atomic Ions*, Vol. 296, NATO Advanced Study Institute Series B: Physics. Plenum Publishing Corporation, New York, pp. 271-300 (1992).

[45] S. Doukas, I. Madesis, A. Dimitriou, A. Laoutaris, T. J. M. Zouros and E. P. Benis, Determination of the solid angle and response function of a hemispherical spectrograph with injection lens for Auger electrons emitted from long lived projectile states, *Rev. Sci. Instrum.* **86**, 043111 (2015).

[46] E. P. Benis, S. Doukas, T. J. M. Zouros, P. Indelicato, F. Parente, C. Martins, J. P. Santos and J. P. Marques, Evaluation of the effective solid angle of a hemispherical deflector analyser with injection lens for metastable Auger projectile states, *Nucl. Instrum. Methods Phys. Res. B* **365**, 457-461 (2015).

[47] E. P. Benis, I. Madesis, A. Laoutaris, S. Nanos and T. J. M. Zouros, Experimental determination of the effective solid angle of long-lived projectile states in zero-degree Auger projectile spectroscopy, *J. Electron Spectrosc. and Relat. Phenom.* **222**, Supplement C, 31-39 (2018).

[48] D. H. Lee, Electron–electron interactions in ion-atom collisions studied by projectile state-resolved Auger electron spectroscopy, Ph.D. dissertation, Kansas State University (1990), (unpublished).

[49] E. P. Benis, A novel high-efficiency paracentric hemispherical spectrograph for zero-degree Auger projectile spectroscopy, Ph.D. dissertation, Dept. of Physics, University of Crete (2001), (unpublished).

[50] J. Doerfert, E. Träbert, A. Wolf, D. Schwalm and O. Uwira, Precision measurement of the electric dipole intercombination rate in C^{2+}, *Phys. Rev. Lett.* **78**, 4355-4358 (1997).

[51] E. Träbert, A. Wolf and G. Gwinner, Measurement of EUV intercombination transition rates in Be-like ions at a heavy-ion storage ring, *Phys. Lett. A* **295**, 44-49 (2002).

[52] A. Müller, S. Schippers, R. A. Phaneuf, A. L. D. Kilcoyne, H. Bräuning, A. S. Schlachter, M. Lu and B. M. McLaughlin, Fine-structure resolved photoionization of metastable Be-like ions C III, N IV, and O V, *J. Phys: Conf. Ser.* **58**, 383-386 (2007).

[53] N. Stolterfoht, P. D. Miller, H. F. Krause, Y. Yamazaki, J. K. Swenson, R. Bruch, P. F. Dittner, P. L. Pepmiller and S. Datz, Surgery of fast, highly charged ions studied by zero-degree Auger spectroscopy, *Nucl. Instrum. Methods Phys. Res. B* **24/25**, 168-172 (1987).

[54] S. W. J. Scully, A. Aguilar, E. D. Emmons, R. A. Phaneuf, M. Halka, D. Leitner, J. C. Levin, M. S. Lubell, R. Püttner, A. S. Schlachter, A. M. Covington, S. Schippers, A. Müller and B. M. McLaughlin, K-shell photoionization of Be-like carbon ions: experiment and theory for C^{2+}, *J. Phys. B* **38**, 1967-1975 (2005).

[55] M. M. A. Shorman, M. F. Gharaibeh, J. M. Bizau, D. Cubaynes, S. Guilbaud, N. E. Hassan, C. Miron, C. Nicolas, E. Robert, I. Sakho, C. Blancard and B. M. McLaughlin, K-shell photoionization of Be-like and Li-like ions of atomic nitrogen: experiment and theory, *J. Phys. B* **46**, 195701 (2013).

[56] A. Müller, S. Schippers, R. A. Phaneuf, S. W. J. Scully, A. Aguilar, C. Cisneros, M. F. Gharaibeh, A. S. Schlachter and B. M. McLaughlin, K-shell photoionization of Be-like boron (B^+) ions: experiment and theory, *J. Phys. B* **47**, 135201 (2014).

[57] B. M. McLaughlin, J.-M. Bizau, D. Cubaynes, S. Guilbaud, S. Douix, M. M. A. Shorman, M. O. A. E. Ghazaly, I. Sakho and M. F. Gharaibeh, K-shell photoionization of O^{4+} and O^{5+} ions: experiment and theory, *MNRAS* **465**, 4690-4702 (2017).

[58] M. H. Chen, B. Crasemann and H. Mark, Deexcitation of light Li-like ions in the $1s2s2p$ state, *Phys. Rev. A* **27**, 544-547 (1983).

[59] D. Schneider, R. Bruch, W. Butscher and W. H. E. Schwarz, Prompt and time-delayed electron decay-in-flight spectra of gas-excited carbon ions, *Phys. Rev. A* **24**, 1223-1236 (1981).

[60] D. Röhrbein, T. Kirchner and S. Fritzsche, Role of cascade and Auger effects in the enhanced population of the $C^{3+}(1s2s2p\,^4P)$ states following single-electron capture in $C^{4+}(1s2s\,^3S)$-He collisions, *Phys. Rev. A* **81**, 042701 (2010).

[61] E. P. Benis, T. J. M. Zouros, T. W. Gorczyca, A. D. González and P. Richard, Erratum: Elastic resonant and nonresonant differential scattering of quasifree electrons from $B^{4+}(1s)$ and $B^{3+}(1s^2)$ ions [*Phys. Rev. A* **69**, 052718 (2004)], *Phys. Rev. A* **73**, 029901 (2006).

[62] D. H. Lee, T. J. M. Zouros, J. M. Sanders, P. Richard, J. M. Anthony, Y. D. Wang and J. H. McGuire, K-shell ionization of O^{4+} and C^{2+} ions in fast collisions with H_2 and He targets, *Phys. Rev. A* **46**, 1374-1387 (1992).

[63] E. P. Benis, S. Doukas and T. J. M. Zouros, Evidence for the non-statistical population of the $1s2s2p\,^4P$ metastable state by electron capture in 4 Mev collisions of $B^{3+}(1s2s\,^3S)$ with H_2 targets, *Nucl. Instrum. Methods Phys. Res. B* **369**, 83-86 (2016).

[64] T. Kirchner (2016), private communications.

[65] T. J. M. Zouros, D. H. Lee and P. Richard, Projectile 1s→2p excitation due to electron-electron interaction in collisions of F^{6+} and O^{5+} ions with He and H_2 targets, *Phys. Rev. Lett.* **62**, 2261-2264 (1989).

[66] J. P. Santos, F. Parente, M. C. Martins, P. Indelicato, E. P. Benis, T. J. M. Zouros and J. Marques, Radiative transition rates of $1s2s(^3S)3p$ levels for Li-like ions with $5 \le Z \le 10$, *Nucl. Instrum. Methods Phys. Res. B* **408**, Supplement C, 100-102 (2017).